IEEE Photonics Journal
An IEEE Photonics Society Publication

Open Access

Rayleigh-Scattering-Induced RIN and Amplitude-to-Phase Conversion as a Source of Length-Dependent Phase Noise in OEOs

Volume 5, Number 2, April 2013

Andrew Docherty
Curtis R. Menyuk
James P. Cahill
Olukayode Okusaga
Weimin Zhou

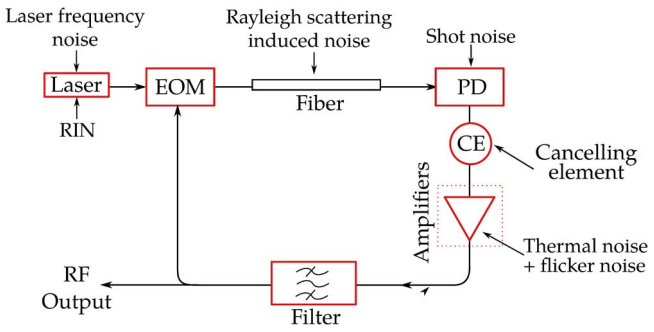

DOI: 10.1109/JPHOT.2013.2250940
1943-0655/$31.00 ©2013 IEEE

IEEE photonics SOCIETY

IEEE

Rayleigh-Scattering-Induced RIN and Amplitude-to-Phase Conversion as a Source of Length-Dependent Phase Noise in OEOs

Andrew Docherty,[1] Curtis R. Menyuk,[1] James P. Cahill,[2] Olukayode Okusaga,[2] and Weimin Zhou[2]

[1]University of Maryland Baltimore County, Baltimore, MD 21250 USA
[2]Army Research Laboratory, Adelphi, MD 20783 USA

DOI: 10.1109/JPHOT.2013.2250940
1943-0655/$31.00 ©2013 IEEE

Manuscript received January 21, 2013; revised February 15, 2013; accepted February 19, 2013. Date of publication March 7, 2013; date of current version March 22, 2013. Corresponding author: A. Docherty (e-mail: docherty@gmail.com).

Abstract: Optoelectronic oscillators (OEOs) are hybrid RF-photonic oscillators that promise to be environmentally robust frequency sources with very low phase noise. Recent experiments have shown that the excess flicker phase noise in these systems grows with the length of the optical fiber loop. In this paper, we detail a mechanism for this length-dependent flicker noise in which Rayleigh-scattering-induced amplitude noise in the optical fiber combines with amplitude-to-phase noise conversion in the nonlinear electronic components. We derive an analytic model of the loop noise that includes these effects and verify this model by comparing it to numerical calculations and experimental results.

Index Terms: Optoelectronic oscillators (OEOs), flicker noise, optical scattering noise.

1. Introduction

Optical fiber-length-dependent flicker phase noise has been identified as a major limit to the reduction of phase noise in optoelectronic oscillators (OEOs) [1]. Due to the increase in the system Q as the length of the optical fiber is increased, the radio-frequency (RF) phase noise of an OEO should decrease with increasing fiber length; however, in some experimental systems, this expected decrease is not observed at lower frequencies. Similar effects have been observed in the duplex transfer of frequencies over optical fiber [2], [3]. The low-frequency phase noise is a critical measure of the stability of oscillators; therefore, identifying the sources of this effect and mitigating them is important to increase the performance of OEOs and other RF photonic systems that use long lengths of optical fiber.

Sources of flicker noise in the RF components of the system have been extensively studied [4], [5]. By contrast, flicker noise that comes from the optical parts of the system have only recently been investigated. A principal source of flicker noise that can affect the OEO performance is the laser; it has been demonstrated experimentally that laser frequency noise can convert directly to RF phase noise via the fiber dispersion [6] and that laser relative intensity noise (RIN) can be converted through amplitude-to-phase (AM-PM) conversion in the photodetector to RF phase noise [7]. In addition, laser frequency noise can be converted to RF phase noise scattering from endfaces, splices, and imperfections in the optical fiber [7], [8].

Experimental evidence indicates that these sources of flicker noise are not the only source of length-dependent phase noise in the optical domain. Recent experiments have shown that in our OEO system, the use of a low-dispersion fiber does not reduce the flicker phase noise, and furthermore, the flicker noise is dependent on the optical power in the fiber as well as its length [1]. It was recently demonstrated that guided entropy mode Rayleigh scattering (GEMRS) gives rise to an effective RIN at the end of a 6-km optical fiber that is a factor of up to 100 times larger than the input RIN. This scattering noise source has been measured to have a frequency spectrum that is characteristic of an inelastic Rayleigh scattering process whose characteristic length equals the fiber core diameter [9].

AM-PM conversion occurs in many different electronic systems. Any components with a nonlinear phase response will give rise to AM-PM conversion, particularly when the components are operated in saturation, as is the case in oscillators. The main nonlinear components in the OEO are the photodetector, the RF amplifier, and the electrooptic modulator (EOM). AM-PM conversion in photodetectors is known to be an important source of phase noise in mode-locked oscillators that produce short output pulses [10], as well as in OEOs [7]. In addition, AM-PM conversion has also been shown to occur in detuned resonators [11].

Previous studies have theoretically calculated the total signal power of signal and noise in an OEO loop but have not included AM-PM conversion [12]–[16]. In previous work, we have shown that AM-PM conversion, along with low-frequency scattering in the optical fiber, can explain the length-dependent flicker noise in our experiments [17]. In this paper, we develop a detailed system-level model of these phenomena that uses a Saleh model [18], a simple nonlinear model with a nonlinear phase response, to model the AM-PM conversion in the RF domain. We treat the fiber-induced scattering noise as a noise source with a frequency response taken from our experiments. We show that it is possible in principle to significantly reduce this contribution to the flicker noise in the OEO by canceling the AM-PM conversion with a nonlinear component having a properly tuned phase response. Previous studies have found operating points with zero AM-PM conversion in photodetectors [10], [19] and have demonstrated that, at this operating point, the flicker phase noise in OEOs is reduced [7]. We have found experimentally, as have others [7], that modulating the input optical signal can also reduce the length-dependent flicker noise; this modulation appears to disrupt the Rayleigh scattering in the fiber. We calculate the maximum possible advantage that can be obtained if the scattering is eliminated. In addition, we design a nonlinear component to cancel the effects of AM-PM conversion in the loop. We demonstrate theoretically that with the compensating component, the phase noise is reduced to the same level as when there is no scattering.

This paper is organized as follows: In Section 2, we discuss the OEO and our experimental setup. In Section 3, we review the Saleh model for a saturable nonlinearity and for multiple-element models of nonlinearity. We calculate the combined amplitude-to-amplitude (AM-AM) and AM-PM response for a multiple-element Saleh model and demonstrate that a two-element model yields a zero AM-PM conversion at a specific operating point. In Section 4, we discuss an empirical model for the scattering-induced amplitude noise of the fiber and develop a loop model of the OEO including AM-PM effects in the photodetector and RF amplifiers. We show that the Rayleigh-scattering-induced RIN is the major contributor to the low-frequency phase noise in the OEO between 1 and 10 kHz from the carrier, and we demonstrate that a nonlinear element inserted into the loop before the amplifiers can be designed to cancel the AM-PM conversion in the loop and reduce the low-frequency phase noise significantly. Section 5 gives the conclusions.

2. OEO Model

The OEO operates as a delay line oscillator with a large delay given by a long length of optical fiber [12]. Here, we model an OEO loop similar to the experimental single-loop OEO of Okusaga *et al.* [9]. This system configuration is illustrated in Fig. 1. In this configuration, the RF signal is modulated onto the fiber by a laser, detected by a photodetector after propagation, and amplified by a bank of three amplifiers. The fundamental tone is filtered to remove harmonics, which completes the loop.

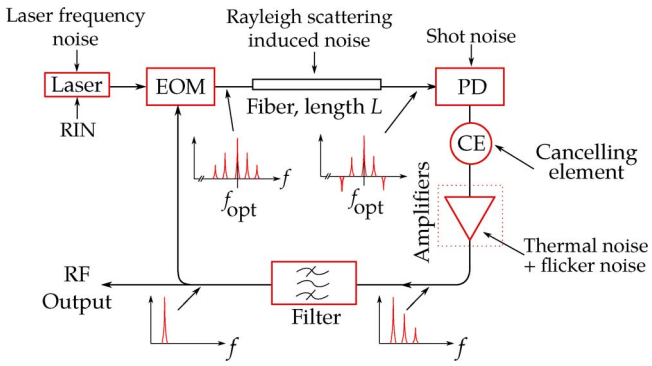

Fig. 1. Schematic of all the basic components of an OEO, including the laser, the EOM, the optical fiber, the photodetector (PD), the RF amplifier, and the RF filter. The noise sources associated with each component are indicated.

OEOs have noise sources in both the electronic and optical domains. The noise sources that we consider here include the shot noise in the photodetector, the thermal noise in the amplifier, the laser frequency and RIN, and the Rayleigh-scattering-induced amplitude noise in the optical fiber. The phase noise in the loop is due to the direct contribution of the phase noise sources and the indirect contribution of amplitude noise that is converted to phase noise in the RF domain. The largest noise source in the OEO at any frequency will depend on the exact specifications of different components used in the loop. While the dominant noise source will change, there will be a contribution from all noise sources.

To demonstrate this claim, and to show the relative contribution of different sources of phase noise in our system, we have developed a system-level model of the OEO. This system model includes an empirical model for the Rayleigh-scattering-induced RIN noise in the optical fiber, a nonlinear model for the RF domain AM-PM conversion in the photodetector and RF amplifiers, and a noise model for the amplitude and phase noise in the OEO due to these effects.

3. Saleh Model for a Saturable Nonlinearity

Complex component-level models for RF amplifiers exist, but they are highly complex as even the simplest amplifier consists of many components with many sources of nonlinearity. These complex models would not be appropriate for modeling the OEO, even if we had available a detailed component-level design, and we do not. We therefore model the nonlinear components each with a multi-element Saleh model that includes both saturable amplification and an AM-PM response. The Saleh model was originally developed to model traveling wave tube amplifiers [18] but is now also used to model solid state power amplifiers [20]. In this paper, we model both the RF amplifier bank and the photodetector.

To model complex nonlinear responses, we concatenate multiple Saleh elements. Each additional element adds parameters and increases the complexity of the response that can be modeled. Each individual Saleh element corresponds to a simple canonical nonlinear response with a saturation power and phase response. A multi-element Saleh model can therefore be considered to be built up from individual Saleh elements in the same manner as the Sellmeier expansion of the material dispersion is built up from a sum of individual Lorentzian models. While single-element Saleh models have been used for a long time in the RF community, multi-element Saleh models have not been widely used. We will show that two-element Saleh models have sufficient complexity to model the OEO's response to noise at the operating point of the OEO. These models also have the benefit that they can be used for input powers over many decades. Other models such as a complex power series have no physical interpretation, and the gain response diverges outside a small range of input powers [20].

We model the RF oscillation in the OEO as a voltage phasor $v(t)$. The real RF output voltage in the loop oscillating at the frequency ω_0 is then $v_{RF}(t) = v(t)\exp(j\omega_0 t) + \text{c.c.}$ The phasor including

both amplitude noise $\alpha(t)$ and phase noise $\phi(t)$ is then written as

$$v(t) = v_0[1 + \alpha(t)]\exp[j\phi(t)]. \tag{1}$$

Representing the relative amplitude noise at the input to any component as $\alpha_{\text{in}}(t)$ and the output amplitude noise as $\alpha_{\text{out}}(t)$, we can write the effect of gain compression as

$$\alpha_{\text{out}}(t) = \gamma_{\text{am}}\alpha_{\text{in}}(t) \tag{2}$$

where γ_{am} is the AM-AM conversion coefficient. The output phase noise is the sum of the input phase noise and the phase noise converted from amplitude noise by AM-PM conversion, which may be written as

$$\phi_{\text{out}}(t) = \gamma_{\text{pm}}\alpha_{\text{in}}(t) + \phi_{\text{in}}(t) \tag{3}$$

where γ_{pm} is the AM-PM conversion coefficient.

The linearized parameters γ_{am} and γ_{pm} are calculated by linearizing the response about the large-signal operating voltage v_0. For a general nonlinear gain response given by $G(v)$, we find

$$\gamma_{\text{am}}(v_0) = 1 + \text{Re}\left[\frac{v_0}{G(v_0)}G'(v_0)\right] \tag{4a}$$

$$\gamma_{\text{pm}}(v_0) = \text{Im}\left[\frac{v_0}{G(v_0)}G'(v_0)\right] \tag{4b}$$

where $G'(v) = dG/dv$. We note that the AM-PM conversion coefficient $\gamma_{\text{pm}}(v)$ can be directly related to the voltage-dependent phase response of the component $\phi(v)$ that is also used to measure AM-PM conversion [19]

$$\gamma_{\text{pm}}(v) = v\frac{\text{d}\phi}{\text{d}v}. \tag{5}$$

In the following sections, we review the single- and multiple-element Saleh models.

3.1. Single-Element Saleh Model

The complex gain of a single-element Saleh model is given by the equation [20]

$$G(v) = G_0\left[\frac{1}{1 + (v/u^{(1)})^2} + j\frac{c(v/u^{(2)})}{1 + (v/u^{(2)})^2}\right] \tag{6}$$

where v is the magnitude of the input voltage to the component, G_0 is the small-signal gain, c is the phase coefficient, and $u^{(1)}$ and $u^{(2)}$ are related to the saturation voltage of the model. In this paper, we have set $u = u^{(1)} = u^{(2)}$, which is the saturation voltage. Now, using (6) and (4), the AM-AM and AM-PM conversion coefficients for the Saleh model are given by

$$\gamma_{\text{am}}(v) = \frac{2}{1 + (v/u)^2} - \frac{1}{1 + c^2(v/u)^2} \tag{7a}$$

$$\gamma_{\text{pm}}(v) = \frac{cv/u}{1 + c^2(v/u)^2}. \tag{7b}$$

The Saleh model of (6) can be parameterized by the phase coefficient c. The response of the model changes qualitatively for different values of c. The magnitude of the gain $|G(v)|$ decreases monotonically for $c^2 < 2$, whereas for $c^2 > 2$, the gain peaks at $v = u/(1 - 2c^2)$ before decreasing. The output voltage peaks at $v = u(1 - 1/c^2)$ when $c^2 < 1/2$, and conversely, when $c^2 \geq 1/2$, the output voltage increases monotonically. We plot the the normalized gain and the normalized output voltage in these three regions in Fig. 2.

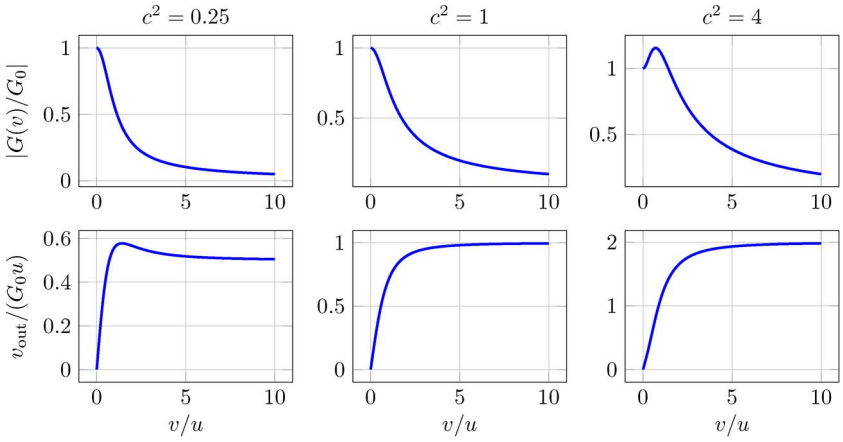

Fig. 2. Normalized gain (top row) and normalized output voltage (bottom row) of the Saleh model of (6) plotted versus the normalized input voltage. The three different values of the phase coefficient c (columns) represent the three qualitatively different regions of the response, for $c^2 < 1/2$, $1/2 \leq c^2 \leq 2$, and $c^2 > 2$.

3.2. Multiple-Element Saleh Models

A multi-element Saleh model can be written compactly as

$$G_m(v) = G_0 \prod_{k=1}^{m} G_m^{(k)}(v_k) \tag{8}$$

where G_0 is the small-signal gain. The gain of the individual elements is given by

$$G_m^{(k)}(v) = \frac{1 + jc_k(v/u_k)}{1 + (v/u_k)^2} \tag{9}$$

and the magnitude of the intermediate voltages at the input of each element is given by

$$v_k = \left| G_m^{(k-1)}(v_{k-1}) v_{k-1} \right| \tag{10}$$

where we define $v_1 = v$ as the input voltage. Each extra element of the chained system adds two parameters, namely, the phase response and the nonlinear saturation voltage. The gain at each stage combines with the saturation voltage of the next stage, so that only the gain of the final component is an independent parameter.

The general expression for the AM-AM and AM-PM coefficients of the multi-element model of (8) is given by

$$\gamma_{\text{am,tot}}(v) = \prod_{k=1}^{m} \gamma_{\text{am},k}(v_k) \tag{11a}$$

$$\gamma_{\text{pm,tot}}(v) = \sum_{k=1}^{m} \prod_{l=1}^{k-1} \gamma_{\text{am},l}(v_l) \gamma_{\text{pm},k}(v_k) \tag{11b}$$

where $\gamma_{\text{am},k}$ and $\gamma_{\text{pm},k}$ are the AM-AM and AM-PM coefficients of the kth element and can be calculated from the element gain $G_m^{(k)}$ using (7). The formula of (11) can be intuitively understood. The amplitude fluctuation at the output of an element in the system affects the gain of the next element in the chain. The phase fluctuation at the output of an element adds directly to the signal as the gain response is only affected by the magnitude of the input signal.

In the case of a two-element system, the concatenated system has three normalized parameters that govern the qualitative behavior of the response, namely, c_1, the normalized phase parameter

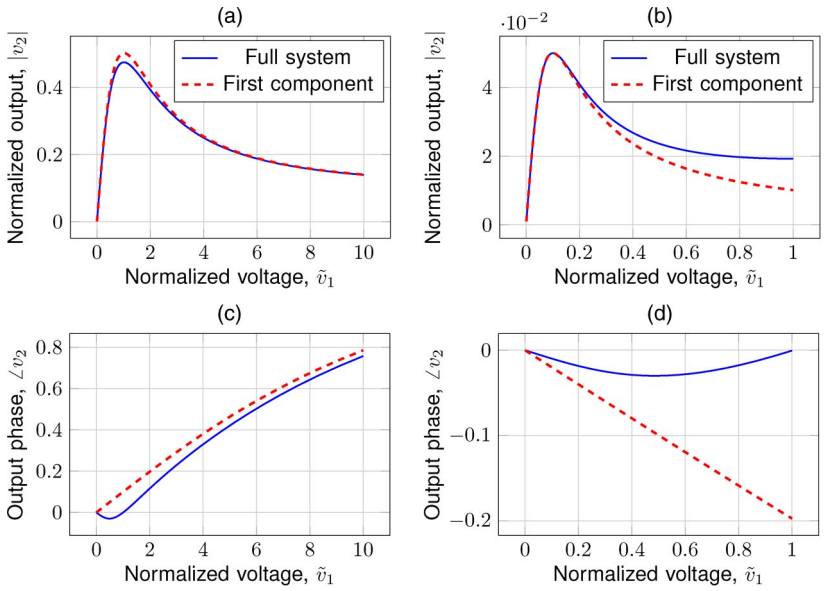

Fig. 3. Normalized output voltage magnitude (top row) and phase (bottom row) of the combined Saleh model of (6) plotted versus the normalized input voltage. The nonlinear response is plotted for the two-component system (blue line), as well as for the component with the smallest saturation voltage (red dashed line). The first component has a saturation voltage of one. The phase coefficients used are $c_1 = 0.1$ and $c_2 = -0.2$. (a) $u_2 = 2u_1$. (b) $u_2 = 0.1u_1$. (c) $c_2 = -0.2$. (d) $u_2 = 0.1u_1$.

from the first component; c_2, the normalized phase parameter from the second component; and u_2, the saturation voltage of the second component.

To illustrate the behavior of the two-element model, we define normalized voltages

$$\tilde{v}_i = v_i/u_i \tag{12}$$

where $\tilde{v}_1 = |v|/u_1$ is the normalized input voltage. We show the normalized output voltage versus the normalized input voltage for different values of the saturation voltage u_2 in Fig. 3. Typically, the gain response of a series of concatenated components is governed by the component with the lowest saturation voltage, as that component will saturate before the others. We illustrate this behavior for our two-component system. The case that the saturation voltage of the second component is much greater than the saturation voltage of the first component, i.e., $u_2 \gg u_1$, is shown in Fig. 3(a), whereas the case that the saturation voltage of the second component is much less than that for the first component, i.e., $u_2 \ll u_1$, is shown in Fig. 3(b). The figures show the response over a range of input voltages up to 10 times the smallest saturation voltage of all components. While the gain response is determined by the component with the smallest saturation voltage, the phase is considerably changed with the addition of the second component, and in particular, there can be a point where the derivative of the phase is zero. In addition, the system phase response is independent of the saturation of the second component and is identical, apart from the axis scale, for both cases, as shown in Fig. 3(c) and (d).

The total AM-AM and AM-PM conversion for the two-component system can be calculated using (4) and (8), which gives the AM-AM and AM-PM coefficients as

$$\gamma_{\text{am}} = \left(\frac{2}{1+\tilde{v}_2^2} - \frac{1}{1+c_2^2\tilde{v}_2^2}\right)\left(\frac{2}{1+\tilde{v}_1^2} - \frac{1}{1+c_1^2\tilde{v}_1^2}\right) \tag{13a}$$

$$\gamma_{\text{pm}} = \frac{c_1\tilde{v}_1}{1+c_1^2\tilde{v}_1^2} + \left(\frac{2}{1+\tilde{v}_1^2} - \frac{1}{1+c_1^2\tilde{v}_1^2}\right)\frac{c_2\tilde{v}_2}{1+c_2^2\tilde{v}_2^2} \tag{13b}$$

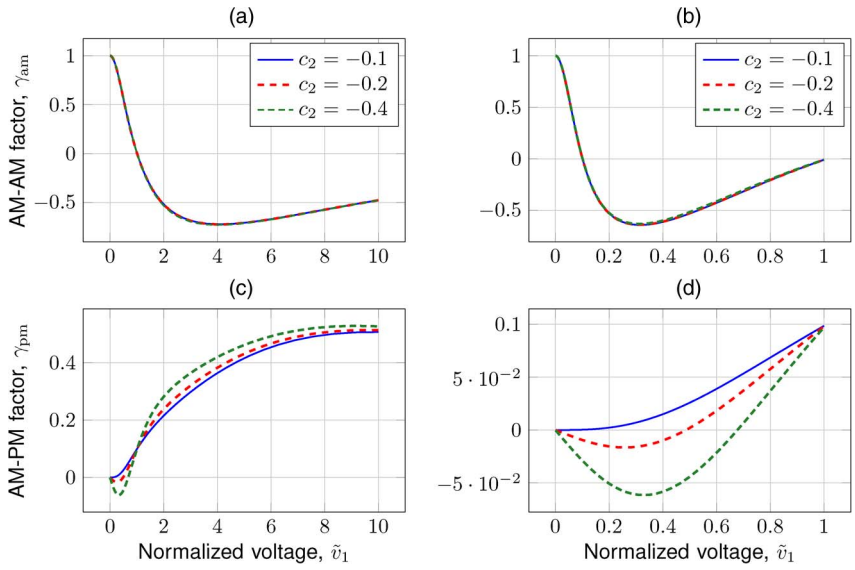

Fig. 4. AM-AM coefficient γ_{am} (top row) and AM-PM coefficient γ_{pm} (bottom row) of the combined Saleh model of (6) plotted versus the normalized input voltage. (a) $u_2 = 2$. (b) $u_2 = 0.1u_1$. (c) $u_2 = 2$. (d) $u_2 = 0.1$.

where the subscripts 1 and 2 indicate the parameters of the first and second Saleh elements in the chain.

We can simplify this expression assuming that c_1 and c_2 are small and of the same order; we expand (13b) to first order in c_1 and c_2

$$\begin{aligned}\gamma_{pm} &\simeq c_1\tilde{v}_1 - c_2\tilde{v}_2 + \frac{2c_2\tilde{v}_2}{1+\tilde{v}_1^2} \\ &\simeq c_1\tilde{v}_1 + \frac{c_2\tilde{v}_1\left(1-\tilde{v}_1^2\right)}{u_2\left(1+\tilde{v}_1^2\right)^2}\end{aligned} \tag{14}$$

where we have used the approximate expression $\tilde{v}_2 \simeq 1/(1+\tilde{v}_1^2)v_1/u_2$. We can then solve this expression to find the normalized input voltage, where there is zero AM-PM conversion, i.e., $\gamma_{pm} = 0$, to obtain

$$\tilde{v}_1^2 = \frac{c_2}{2c_1u_2} \pm \frac{\sqrt{c_2(c_2-8c_1u_2)}}{2c_1u_2} - 1. \tag{15}$$

Here, we see that there exists a voltage where the AM-PM coefficient for the two-component system is zero when $c_1 > 0$ and $c_2 < -c_1u_2$ or $c_2 > 8c_1u_2$ and, similarly, when $c_1 < 0$ and $c_2 > -c_1u_2$ or $c_2 < 8c_1u_2$. However, (15) only holds for small c_1 and c_2; for larger phase coefficients, we need to solve $\gamma_{pm}(v_0) = 0$ numerically using the original equation (13b).

In Fig. 4, we show the AM-AM and AM-PM response of systems in one of two sets of operating conditions. The first set is where the second component saturates at a much lower voltage than the first, i.e., $u_1 \ll 1$, and the second set is where the second component saturates at a higher voltage than the first, i.e., $u_1 \gg 1$. In the first model, we used $u_1 = 0.1$, and in the second, $u_1 = 2$, as was the case for the results in Fig. 3. The AM-PM coefficient does not depend on the saturation voltage of the second component, and therefore, the entire AM-PM response and the location of the AM-PM zero can be changed by the phase of the second component independently of the gain response.

Higher order multi-element models can be constructed. Both the gain and phase responses become increasingly more complicated, but nonetheless, the Saleh models remain tractable as individual elements and can be considered as such. In addition, they have a well-controlled amplitude

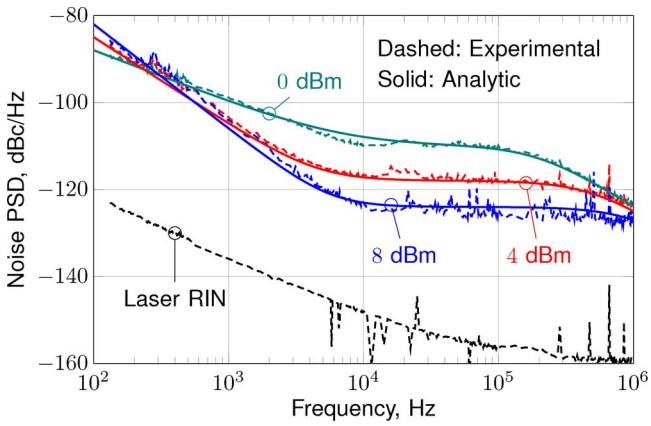

Fig. 5. Comparison of the experimentally measured and modeled PSD after 6 km of propagation, using (16) and the parameters in Table 1. In addition, shown is the laser RIN that was measured before propagation through an optical fiber.

and phase response over many decades of input power and can be chosen to fit experimental data very well.

4. Results

In this section, we describe the OEO loop model that we use to model our OEO, including the scattering noise. We give an empirical model for the PSD of the scattering-induced amplitude noise. We measure the complex gain response of the photodetector and the RF amplifier bank, calculate the AM-AM and AM-PM responses, and fit these to a multi-element Saleh model. Finally, we calculate the loop phase noise with the scattering noise and show the reduction that could be expected when the scattering-induced amplitude noise is removed. In addition, we design an AM-PM canceling element to be placed before the amplifier block with a simple phase response that significantly reduces the loop AM-PM at the operating point of the OEO. This cancelling element is a single-element Saleh response with a specific phase coefficient.

4.1. Scattering-Induced Amplitude Noise

Recent experimental measurements show that the close-in amplitude noise of an optical signal after propagating through fiber is much greater than the RIN noise of the laser and has a shape characteristic of a Rayleigh scattering process [9]. The PSD of the measured scattering noise does not fit well a summation of powers of f. We have found that a good match to the experimentally measured PSD is given by the sum of a two f^{α} noise sources, one of which is multiplied by a factor representing the frequency response of Rayleigh scattering

$$S_{\text{scatt}}(f) = c_1 f^{\alpha_1} + c_2 f^{\alpha_2} \frac{f^2}{f^2 + \Gamma^2/4} \tag{16}$$

where α_i and c_i with $i = 1, 2$ are the exponents and strengths of the noise sources, respectively; and Γ is the bandwidth of the Rayleigh scattering process. The experimental PSD for the amplitude noise measured after 6 km of a single-mode fiber (SMF) using a DFB laser light source, along with the theoretical PSD using (16), is shown in Fig. 5. We also show the fitted analytic PSD given in (16) using the values of the parameters given in Table 1.

4.2. AM-PM Conversion in the Photodiode and the RF Amplifier

Both the photodetector and the RF amplifier are complicated devices and have many nonlinear processes that determine the magnitude and phase response. In modeling them, we only attempt to

TABLE 1

Noise parameters of best fit for transmitted intensity noise through 6 km of SMF

	Optical Power		
Parameter	0 dBm	4 dBm	8 dBm
c_1	4×10^{-7}	3.2×10^{-5}	4×10^{-4}
c_2	0.4	0.4	0.4
α_1	-1.2	-2	-2.4
α_2	-2	-2	-2
Γ	400 kHz	1 MHz	2 MHz

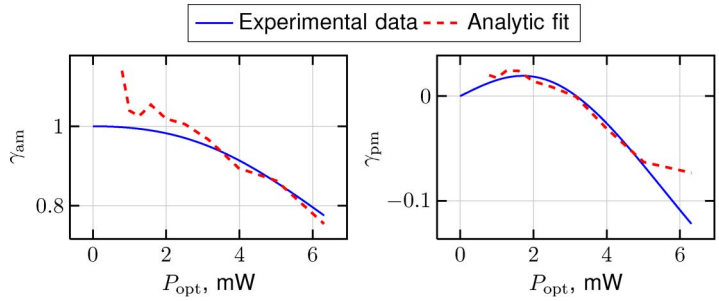

Fig. 6. AM-AM and AM-PM coefficients of the DSC30 photodetector versus the average input optical power. We compare the experimentally measured values to the two-element Saleh model that we use.

capture the first-order behavior of the components, in particular, the saturation power and the same magnitude of AM-PM conversion.

We now use the concatenated Saleh model from the previous section to model the measured gain and phase response of the photodetector used in the OEO, a Discovery Semiconductor DSC30. To measure the phase response, a 1.55-μm laser was AM modulated at 10 GHz with close to 100% modulation, and the output of the photodetector was attached to a network analyzer. The phase of the output RF signal of the photodiode was measured at bias voltages of 4, 6, and 8 V. The slope of this phase versus power graph can be used to estimate the AM-PM coefficient using (5).

We model the photodiode with an empirical model of the nonlinear responsivity of the photodetector

$$I_{\rm out} = R(P_{\rm opt})P_{\rm opt} \tag{17}$$

where $P_{\rm opt}$ is the optical power. This nonlinear responsivity is a two-element Saleh model, which is given by

$$R(P_{\rm opt}) = \rho_0 \left[\frac{1 + jc_2 P_2/P_{\rm sat}}{1 + (P_2/P_{\rm sat})^2}\right]\left[\frac{1 + jc_1 P_{\rm opt}/P_{\rm sat}}{1 + (P_{\rm opt}/P_{\rm sat})^2}\right] \tag{18}$$

where

$$P_2 = \frac{\left[1 + c_1^2 (P_{\rm opt}/P_{\rm sat})^2\right]^{1/2}}{1 + (P_{\rm opt}/P_{\rm sat})^2} P_{\rm opt}. \tag{19}$$

The parameters used were $\rho_0 = 0.7$, $c_1 = 0.73$, $c_2 = 1.75$, and $P_{\rm sat} = 0.01$ W. We can match the experimentally measured AM-AM and AM-PM coefficients above approximately 2 mW, as shown in Fig. 6. The AM-AM coefficient diverges in the measured data below 2 mW as the measured gain decreases. However, this effect would increase the relative noise level by up to 10%, which is well within the expected error of our estimate of the system parameters.

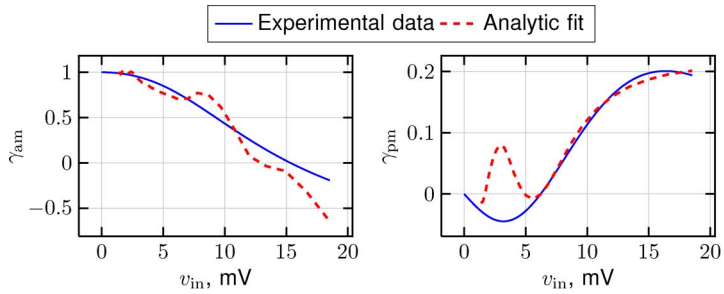

Fig. 7. AM-AM and AM-PM coefficients of the three combined AML RF amplifiers versus the average input optical power. We compare the experimentally measured values to the one-element Saleh model that we use for the entire amplifier bank.

The phase response of the three AML3 low noise 10-GHz power amplifiers used in our OEO configuration has been measured by applying a 10-GHz RF signal to the input of the RF amplifier block. A network analyzer attached to the output of the three amplifiers was used to record the gain and phase versus the RF input power. The responses of these real devices have a complicated phase response. The local slope of the phase response tends to become steeper as the device is driven further into saturation, and the AM-PM conversion of these devices is large when the devices are operated well into saturation. RF amplifiers are often designed to have minimal AM-PM conversion for low input powers; however, in our oscillator, the amplifier is used to control the oscillator amplitude and is therefore in saturation at the operating point. Hence, the AM-PM coefficient of the amplifier is large.

We do not attempt to exactly fit the complex phase response of the real amplifier; instead, we choose the coefficients of a single Saleh model that matches the order of magnitude response of the experimental data in the range of typical input powers of the experimental system, from 7 to 15 mV. This range of input voltages to the amplifier was found to be consistent with the experimental system. The three-element Saleh model for the gain response of the amplifier bank is given by (8) and (9) with the parameters $G_0 = 10^3$, $u_1 = 2.2 \times 10^{-2}$ V, $c_1 = 0.2$, $u_2 = 15.8$ V, $c_2 = 0.43$, $u_3 = 100$ V, and $c_3 = -5.5$. The resulting AM-AM and AM-PM responses for the Saleh model and the experimental system are shown in Fig. 7. The AM-PM response closely matches the experimental system over the range of input voltages of interest. The AM-AM response is more complicated, and the Saleh model does not fit this response as well; however, the AM-AM response governs the loop gain of the amplitude noise and does not contribute to the close-in phase noise of the system.

4.3. OEO Loop Model

We can now model the single OEO loop in Fig. 1 with three nonlinear components, namely, the EOM, the photodiode, and the RF amplifier. The EOM is modeled by the following equation giving the effective fundamental optical power at the input of the photodiode [12]:

$$P_{RF}^{(eff)}(v) = \frac{P_0}{2}\eta \cos\left(\frac{\pi V_B}{V_\pi}\right) J_1\left(\frac{\pi|v|}{V_\pi}\right) \exp(j\angle v) \tag{20}$$

where $V_\pi = 5$ V is the half-wave voltage, $V_B = 5$ V is the bias voltage, $\eta = 0.65$ is the modulation depth, and v is the input voltage to the modulator.

The frequency response of the loop is assumed to be given by the filter, which has the smallest bandwidth of all components in the loop. We take this frequency response to be a Lorentzian with the same bandwidth as the filter. The specific frequency response of the filter is not critical to the low frequency noise of the loop [14]. The filter frequency response is given by

$$F(\omega) = \frac{-j2\pi\Gamma}{\omega - \omega_0 - j2\pi\Gamma} \tag{21}$$

where $\Gamma = 10^6$ Hz is the bandwidth of the filter.

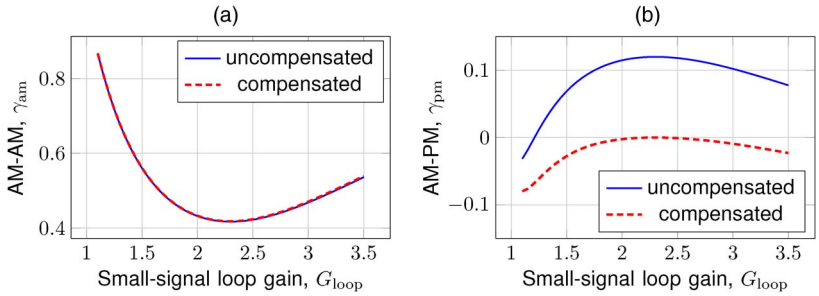

Fig. 8. (a) AM-AM coefficient γ_{am} and (b) AM-PM coefficient γ_{pm} of combined photodetector and RF amplifiers. The coefficients are calculated with respect to the small-signal loop gain. The results for the standard loop and the loop with a compensating element included before the amplifier are shown.

The OEO in Fig. 1 was studied both numerically, using the computational model of Levy *et al.* [14], and analytically, using the theoretical model of [11]. To model the amplitude and phase noise in the oscillator, the small perturbations in phase and amplitude form separate linear loops that interact by only AM-PM conversion. The amplitude and phase noise of the loop can now be written as

$$\alpha_{out}(\omega) = \frac{1}{1 - \gamma_{am}^{(loop)} \exp(j\omega\tau) F(\omega)} \alpha_{in}^{(eff)}(\omega) \tag{22a}$$

$$\phi_{out}(\omega) = \frac{1}{1 - \exp(j\omega\tau) F(\omega)} \phi_{in}^{(eff)}(\omega) \tag{22b}$$

where $\alpha_{in}^{(eff)}$ and $\phi_{in}^{(eff)}$ are the effective input amplitude and phase noise, respectively; and $\gamma_{am}^{(loop)}$ is the AM-AM coefficient of all components in the loop, as calculated by (11).

The effective amplitude noise into the loop $\alpha_{in}^{(eff)}$ includes the contributions from scattering α_{scatt} and thermal noise α_t

$$\alpha_{in}^{(eff)}(\omega) = F(\omega)\left[\gamma_{am}^{(pd)}\gamma_{am}^{(amp)}\alpha_{scatt}(\omega) + \gamma_{am}^{(amp)}\alpha_t(\omega)\right] \tag{23}$$

where γ_{am}^{pd} and γ_{am}^{amp} are the AM-AM conversion coefficients of the photodiode and the amplifier, respectively. The AM-AM coefficients of the multi-element Saleh models used to model the photodetector and the amplifier are calculated using (11).

Similarly, the effective phase noise into the loop $\phi_{in}^{(eff)}$ includes a contribution from thermal noise ϕ_t and from the laser frequency noise ϕ_{LFN}, as well as from scattering noise converted to phase noise by AM-PM in the photodetector and the amplifier

$$\phi_{in}^{(eff)}(\omega) = F(\omega)\left\{\phi_t(\omega) + \phi_{LFN} + \left[\gamma_{pm}^{(pd)} + \gamma_{am}^{(pd)}\gamma_{pm}^{(amp)}\right]\alpha_{scatt}(\omega)\right\} \tag{24}$$

where γ_{pm}^{pd} and γ_{pm}^{amp} are the AM-PM conversions in the photodetector and the amplifier, respectively. The AM-AM coefficient for the modulator, which is the same as the small-signal gain compression given in [12], is

$$\gamma_{am}^{(eom)} = \frac{\pi v}{V_\pi} J_1'\left(\frac{\pi v}{V_\pi}\right) \tag{25}$$

where $J_1'(x) = dJ_1(x)/dx$ is the derivative of the Bessel function.

The scattering noise is modeled by a source with the PSD given by (16). The thermal noise source of the amplifier and the shot noise of the photodetector are modeled as a white noise source with a power spectral density of 4×10^{-18} W/Hz. We assume that the thermal noise is split into amplitude noise α_t and phase noise ϕ_t equally. Additional noise sources included are the length-independent flicker noise as calculated in [13] and the laser frequency noise converted to RF phase noise as calculated in [21]. The optical fiber is modeled as a delay and a loss corresponding to a

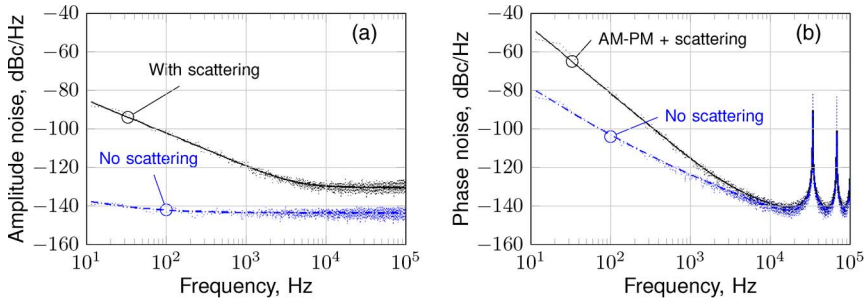

Fig. 9. Theoretical RF phase noise PSD at the output of the OEO. The solid line shows the results including scattering-induced RIN and AM-PM in the photodetector and the RF amplifiers. The dashed line shows the results without the scattering-induced RIN noise source. The dots show the results of the computational model.

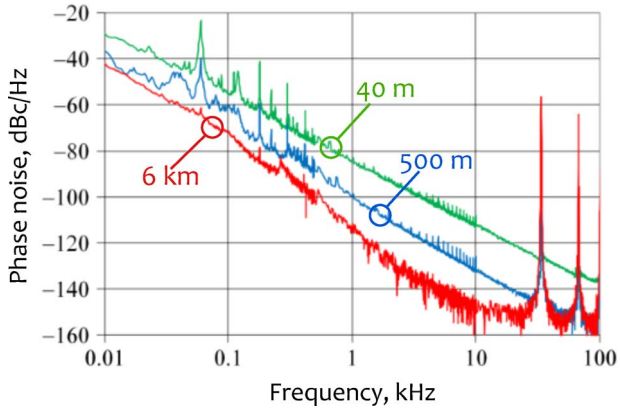

Fig. 10. Experimentally measured RF phase noise in our experimental OEO for different fiber lengths from Adles *et al.* [23].

length of 6 km, taking a loss of 0.2 dB/km. The loss in the RF components is lumped into a loss before the modulator and adjusted to give a specific small-signal loop gain.

The results of the loop model are shown in Fig. 9, using both the analytical formulation given by (22), which is indicated by the solid lines, and a computational model, which is indicated by the dots. The scattering-induced amplitude noise and the AM-PM conversion give a large contribution to the phase noise of the OEO, as can be seen when the scattering noise was removed from the model. In that case, the phase noise drops by around 30 dB at 10 Hz. The next highest source of phase noise in our system was the conversion of laser frequency noise to RF phase noise by dispersion.

This source of phase noise can be compared with the measured phase noise in our OEO system at 6 km, as shown in Fig. 10. The phase noise was measured in a single-loop OEO system using a cross-correlation photonic delay line measurement system [22]. The phase noise level is similar for both the experimental and theoretical systems. The phase noise in the experimental system is somewhat higher at 10 Hz than in our theoretical model. We note that the experimental measurements given are the single-sideband power spectral density. We have therefore plotted the theoretical results as single-sideband measurements to match.

We now demonstrate a theoretical system in which we introduce a compensating nonlinear element before the RF amplifier, as shown in Fig. 1. This element is designed to cancel the AM-PM conversion of the loop at the operating point of the amplifier. The compensating element has a unity small-signal gain and a saturation voltage much larger than the saturation of the amplifier and therefore does not change the gain characteristics of the loop. The gain of this compensating element is given by the single-element Saleh component of (6) with $G_0 = 1$, $c = -1.2$, and $u = 0.1$ V. To calculate the amplitude and phase noise of the loop, we use (22) and replace the

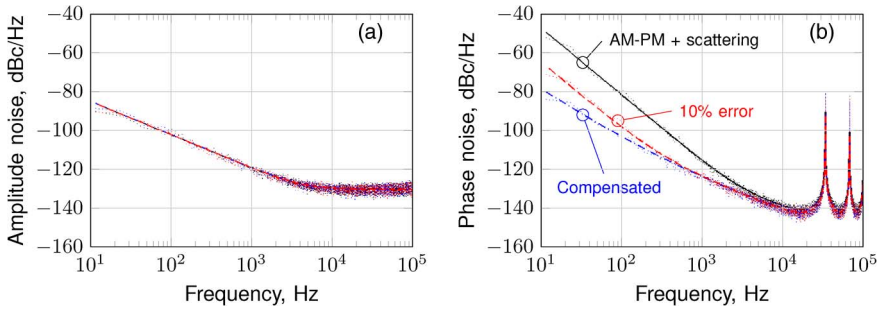

Fig. 11. Theoretical PSD of the (a) RF amplitude noise and (b) RF phase noise at the output of the OEO with the AM-PM canceling component. The solid line shows the results at the nominal loop operating point, the dashed line shows the results when the loop gain is increased by 15%, and the dash-dotted line shows the results when the loop gain is increased by 30%. The dots show the results of the computational model.

AM-AM and AM-PM coefficients of the amplifier with the combined response of the compensating element and the amplifier

$$\gamma_{\text{am}}^{(\text{amp},2)} = \gamma_{\text{am}}^{(\text{ce})}\gamma_{\text{am}}^{(\text{amp})} \tag{26a}$$

$$\gamma_{\text{pm}}^{(\text{amp},2)} = \gamma_{\text{pm}}^{(\text{ce})} + \gamma_{\text{am}}^{(\text{ce})}\gamma_{\text{pm}}^{(\text{amp})}. \tag{26b}$$

The compensating element parameters were chosen to minimize the second equation near the operating point of the OEO, which we take to be the point where the small-signal loop gain is given by $G_{\text{loop}} = 2.3$. The resulting AM-AM and AM-PM coefficients as functions of the small-signal loop gain with and without the compensating element are plotted in Fig. 8. We see that the AM-PM is reduced significantly over a wide operating range when the compensating element is introduced.

We plot the resulting PSD of the amplitude noise of the OEO loop in Fig. 11(a) and the phase noise in Fig. 11(b). This figure shows the noise PSD plotted both from the analytical expressions of (22) and using a numerical simulation of the loop by the method given in Levy *et al.* [14] with a very careful treatment of the gain saturation as described by Rubiola and Brendel [11]. This figure shows that the amplitude noise of the loop is unchanged by the introduction of the compensating element. This result can be compared to the case shown in Fig. 9(a) when the scattering noise source was removed; in this case, the amplitude noise dropped considerably. The phase noise, however, is reduced by around 20 dB. The compensating element will only cancel the phase noise of the loop if the coefficient can be accurately matched to the gain and phase response of the amplifier. However, a mismatch in the parameters of the compensating element under 10% can still result in a considerable reduction in the phase noise in the loop in our system. The effect on phase noise of the compensating element with a change in the phase parameter of 10% is shown in Fig. 11.

5. Conclusion

We have systematically modeled our experimental OEO loop numerically and theoretically including the effects of experimentally-measured scattering noise through the optical fiber and AM-PM conversion in the photodetector and the amplifier. We demonstrated that the scattering-induced amplitude noise and the AM-PM conversion are the largest contributors to the phase noise in our system for frequencies below 10 kHz. We note for different OEO configurations that the balance of noise sources could be different and the scattering-induced noise may not be the dominant noise source. This has been demonstrated in another system where the frequency noise of the laser, which was converted to RF phase noise by fiber dispersion, was shown to dominate [6].

We showed that we can use multiple-element Saleh models to fit the experimentally measured amplitude and phase response of our photodetector and amplifiers over a wide range of powers using two- and three-element models, respectively. This allows an investigation of the nonlinear dynamical effects of the model in addition to the study of the linearized noise response of the

system at the operating point. In addition, the Saleh models are useful for both analytical modeling and numerical simulation as their parameters have a direct physical interpretation.

We demonstrated that a simple nonlinear phase compensating element can be designed to null the AM-PM conversion of the amplifier over a large operating range of the OEO and theoretically gives the same phase noise reduction as does removing the scattering-induced amplitude noise source from the loop. A 10% mismatch in the parameters of this compensating element still results in a reduction in phase noise at 10 Hz of 20 dB. We note that designing an actual electronic device that gives the desired nonlinear response is also not straightforward. The benefit of the Saleh model compensator is that it models a simple saturable nonlinearity with single saturation power. Thus, it should be more straightforward to fabricate a physical device using standard components to match a Saleh compensator than it would be for an arbitrary AM-PM response.

References

[1] O. Okusaga, E. Adles, W. Zhou, C. Menyuk, G. Carter, E. Levy, and M. Horowitz, "Spurious-mode suppression in optoelectronic oscillators," in *Proc. IEEE IFCS*, Newport Beach, CA, USA, Jun. 2010, pp. 539–543.

[2] P. A. Williams, W. C. Swann, and N. R. Newbury, "High-stability transfer of an optical frequency over long fiber-optic links," *J. Opt. Soc. Amer. B*, vol. 25, no. 8, pp. 1284–1293, Aug. 2008.

[3] J. L. Hanssen, S. G. Crane, and C. R. Ekstrom, "One-way temperature compensated fiber link," in *Proc. Joint Conf. IEEE IFCS/Eur. Freq. Time Forum*, San Francisco, CA, USA, May 2011, pp. 1–5.

[4] A. Demir and A. Sangiovanni-Vincentelli, *Analysis and Simulation of Noise in Nonlinear Electronic Circuits and Systems*. Norwell, MA, USA: Kluwer, 1997.

[5] E. Rubiola, *Phase Noise and Frequency Stability in Oscillators*. Cambridge, U.K.: Cambridge Univ. Press, 2008.

[6] K. Volyanskiy, Y. K. Chembo, L. Larger, and E. Rubiola, "Contribution of laser frequency and power fluctuations to the microwave phase noise of optoelectronic oscillators," *J. Lightw. Technol.*, vol. 28, no. 18, pp. 2730–2735, Sep. 2010.

[7] D. Eliyahu, D. Seidel, and L. Maleki, "RF amplitude and phase-noise reduction of an optical link and an opto-electronic oscillator," *IEEE Trans. Microw. Theory Tech.*, vol. 56, no. 2, pp. 449–456, Feb. 2008.

[8] W. Shieh and L. Maleki, "Phase noise of optical interference in photonic RF systems," *IEEE Photon. Technol. Lett.*, vol. 10, no. 11, pp. 1617–1619, Nov. 1998.

[9] O. Okusaga, J. Cahill, A. Docherty, W. Zhou, and C. R. Menyuk, "Guided entropy mode Rayleigh scattering in optical fibers," *Opt. Lett.*, vol. 37, no. 4, pp. 683–685, Feb. 2012.

[10] J. Taylor, S. Datta, A. Hati, C. Nelson, F. Quinlan, A. Joshi, and S. Diddams, "Characterization of power-to-phase conversion in high-speed P-I-N photodiodes," *IEEE Photon. J.*, vol. 3, no. 1, pp. 140–151, Feb. 2011.

[11] E. Rubiola and R. Brendel, *A Generalization of the Leeson Effect*, Apr. 2010, arXiv:1004.5539v1. [Online]. Available: http://arxiv.org/abs/1004.5539

[12] X. S. Yao and L. Maleki, "Converting light into spectrally pure microwave oscillation," *Opt. Lett.*, vol. 21, no. 7, pp. 483–485, Apr. 1996.

[13] E. C. Levy, O. Okusaga, M. Horowitz, C. R. Menyuk, W. Zhou, and G. M. Carter, "Comprehensive computational model of single- and dual-loop optoelectronic oscillators with experimental verification," *Opt. Exp.*, vol. 18, no. 20, pp. 21 461–21 476, Sep. 2010.

[14] E. E. Levy, M. Horowitz, and C. Menyuk, "Modeling optoelectronic oscillators," *J. Opt. Soc. Amer. B*, vol. 26, no. 1, pp. 148–159, Jan. 2009.

[15] Y. K. Chembo, K. Volyanskiy, L. Larger, E. Rubiola, and P. Colet, "Determination of phase noise spectra in optoelectronic microwave oscillators: A Langevin approach," *IEEE J. Quantum Electron.*, vol. 45, no. 2, pp. 178–186, Feb. 2009.

[16] Y. K. Chembo, L. Larger, and P. Colet, "Nonlinear dynamics and spectral stability of optoelectronic microwave oscillators," *IEEE J. Quantum Electron.*, vol. 44, no. 9, pp. 858–866, Sep. 2008.

[17] A. Docherty, C. R. Menyuk, O. Okusaga, and W. Zhou, "Stimulated Rayleigh scattering and amplitude-to-phase conversion as a source of length-dependent phase noise in OEOs," in *Proc. IEEE IFCS*, Baltimore, MD, USA, May 2012, pp. 1–5.

[18] A. Saleh, "Frequency-independent and frequency-dependent nonlinear models of TWT amplifiers," *IEEE Trans. Commun.*, vol. COM-29, no. 11, pp. 1715–1720, Nov. 1981.

[19] A. Joshi and S. Datta, "Dual InGaAs photodiodes having high phase linearity for precise timing applications," *IEEE Photon. Technol. Lett.*, vol. 21, no. 19, pp. 1360–1362, Oct. 2009.

[20] D. Schreurs, M. O'Droma, A. A. Goacher, and M. Gadringer, *RF Power Amplifier Behavioral Modeling*. Cambridge, U.K.: Cambridge Univ. Press, Nov. 2008.

[21] A. Docherty, O. Okusaga, C. R. Menyuk, W. Zhou, and G. M. Carter, "Theoretical investigation of optical fiber-length-dependent phase noise in opto-electronic oscillators," in *Proc. Joint Conf. IEEE IFCS/Eur. Freq. Time Forum*, San Francisco, CA, USA, May 2011, pp. 1–6.

[22] O. Okusaga, W. Zhou, E. Levy, M. Horowitz, G. Carter, and C. R. Menyuk, "Experimental and simulation study of dual injection-locked OEOs," in *Proc. IEEE IFCS*, Apr. 2009, pp. 875–879.

[23] E. J. Adles, A. Docherty, C. Menyuk, G. Carter, O. Okusaga, W. Zhou, E. Levy, A. David, and M. Horowitz, "Loop-length dependent sources of phase noise in optoelectronic oscillators," in *Proc. IEEE IFCS*, Newport Beach, USA, Jun. 2010, pp. 550–553.